The 2010 IEEE/RSJ International Conference on
Intelligent Robots and Systems
October 18-22, 2010, Taipei, Taiwan

On the Z-Width Limitation due to the Vibration Modes of Haptic Interfaces

Jorge Juan Gil, Mildred J. Puerto, Iñaki Díaz and Emilio Sánchez

Abstract— **This paper addresses the effect of internal vibration modes on the stability boundary for haptic rendering. A linear model that includes two vibration modes has been used to characterize one degree-of-freedom of the PHANToM 1.0 haptic interface, and predict the maximum achievable impedances for haptic rendering. The theoretical and experimental results show that the vibration modes of the mechanical interface significantly limit the Z-width of the haptic system.**

Index Terms— **Haptic systems, Stability, Vibration modes**

I. Introduction

Haptic interfaces are becoming very popular as simulation tools in surgery [1], [2], industry [3], and education [4], among many other fields. Implementing a good haptic controller enables the user to obtain a proper tactile interaction with a virtual environment. However, a number of hardware and software limitations have yet to be solved to provide a high degree of realism.

Impedance-based haptic systems usually model a virtual body by means of a virtual spring. To simulate rigid contacts, the virtual stiffness K is set as high as possible. Several studies [5], [6], [7] have found the dependence of passivity and stability limits on factors such as the sampling period, the viscous damping, and time delays. It has been proven that the addition of a virtual damper in parallel with the virtual spring allows the implementation of higher stiffness coefficients before leading to system instability [8], [9], [10], [11], [12]. This beneficial effect is also achieved by increasing the physical damping of the interface [13], [14], [15], [16].

In a haptic interaction with a virtual impedance that consists of a spring K and damping B, the region containing the stable values of these parameters is called the Z-width of the haptic system [17]. The size and shape of this region can be used to compare the performance of different haptic devices. Therefore, a number of control strategies have been developed with the aim of increasing the Z-width of haptic systems, that is, the set of impedances that they can simulate [18], [19], [20], [21], [22]. The boundary of this stability region has been found experimentally in [12], [13]. Furthermore, it is interesting to note that some experimental studies [17], [18], [22] show that it is not possible to implement relatively high virtual damping coefficients. From a certain value of virtual damping B, the critical value of the virtual stiffness K decreases drastically.

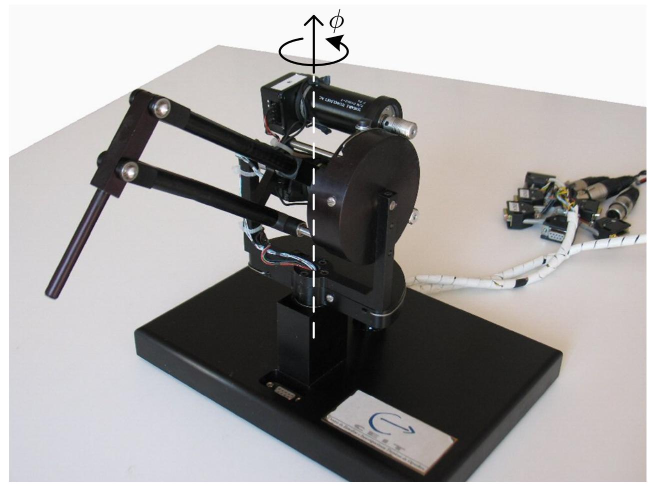

Fig. 1. PHANToM 1.0 haptic interface without stylus and ϕ-axis definition.

This paper shows that the vibration modes of the device are responsible for the limitation of the Z-width. The stable boundary is found by using a theoretical model of the system that includes the vibration modes. This study exhibits that the critical frequency of the system presents a discontinuity as the virtual damping increases, jumping to values above the resonance frequencies of the modes. Experiments that support the theoretical findings are also presented. To extend the validity of this analysis, several time delays have been introduced in both the theoretical models as in the experimental setup.

The well-known PHANToM Premium 1.0 haptic interface (Fig. 1) was used to analyze the influence of the vibration modes on the Z-width of the system. To compute the theoretical stability boundaries, a linear model for the mechanical interface—including the most significant vibration modes—is estimated in Section II. Next, the shapes of the theoretical stability regions are analyzed in Section III, while the experimental regions are shown in Section IV. Finally, some conclusions and future work are reported in the last section.

II. Device Model Identification

This section proposes a linear model for the mechanical interface including its most significant vibration modes. The study is limited to the first degree-of-freedom of the PHANToM (ϕ-axis in Fig. 1). Only the motor that acts on

This work has been supported in part by the Basque Government.

The authors are with the Applied Mechanics Department, CEIT, Paseo Manuel Lardizábal 15, E-20018 San Sebastián (Guipúzcoa), Spain (e-mails: {jjgil,mjpuerto,idiaz,esanchez}@ceit.es) and with the Control and Electronics Department, TECNUN, University of Navarra, Paseo Manuel Lardizábal 13, E-20018 San Sebastián (Guipúzcoa), Spain.

978-1-4244-6676-4/10/$25.00 ©2010 IEEE

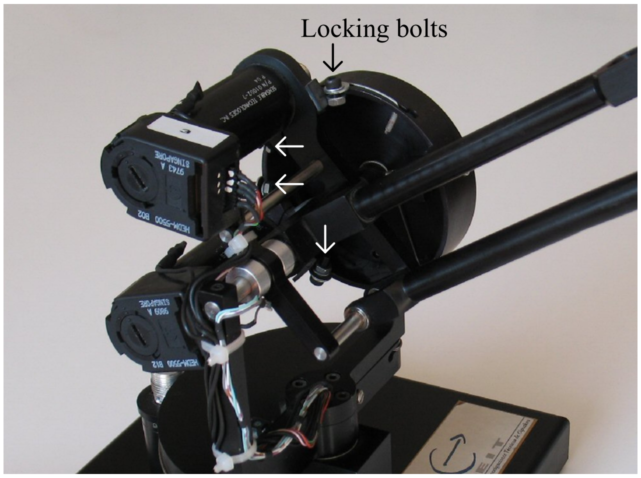

Fig. 2. Four locking bolts are placed on both sides of the non-active motors of the PHANToM to avoid undesired reconfigurations of the device during the experiments.

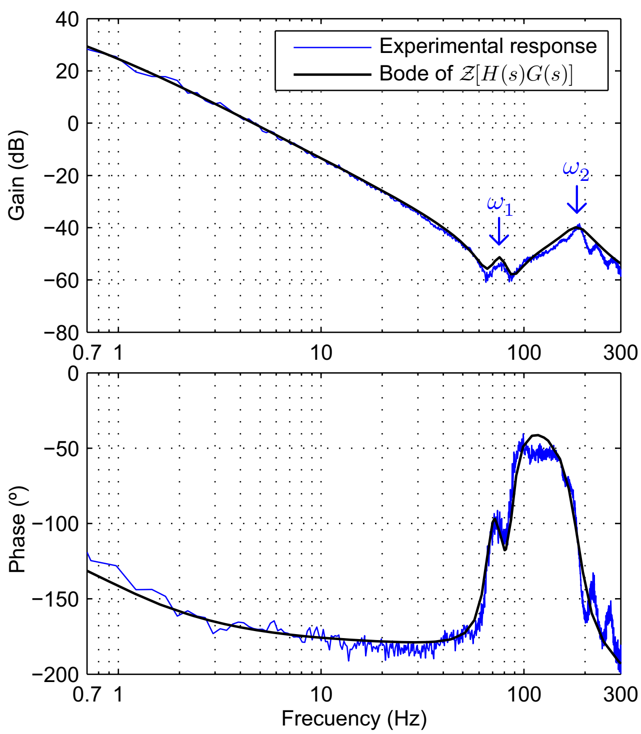

Fig. 3. Experimental (blue line) and theoretical (black line) Bode diagrams for the PHANToM.

this axis is active. To avoid undesired reconfigurations of the rest of the device, the other motors are mechanically locked (Fig. 2). Moreover, the stylus of the PHANToM has been removed to avoid the influence of mobile parts on the device.

The transfer function that characterizes the interface was estimated from the frequency response of the device to a white noise input signal [23]. This type of actuation allows the excitation of a wide range of frequencies and the identification of the first vibration modes of the system.

The white noise signal was generated by a Simulink® block and commanded to the active motor by a dSPACE DS1104 board running at 1 kHz. This board also read the encoder information. The white noise signal successfully excited the system from 0.7 Hz up to 300 Hz over thirty seconds. The lower frequency was set near the limit imposed by the length of the window used in the data analysis (4096 sampling points that allow a smooth frequency response), while the upper limit was set bellow the Nyquist frequency and the bandwidth of the actuators.

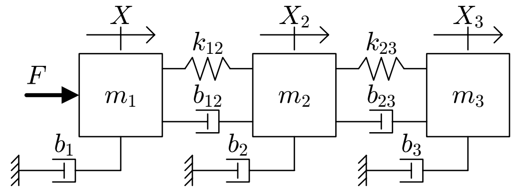

Fig. 4. Mechanical model for the device with two vibration modes.

Fig. 3 shows the frequency response of the PHANToM to the white noise signal. Several vibration modes (at least four) arise below 300 Hz. To manage a relatively simple model, only the first two vibration modes were modeled. The first one (at approximately 80 Hz) is a structural mode of the mechanism, while the second one (close to 200 Hz) is due to the transmission cable. The suggested transfer function for the interface is

$$G(s) = \frac{1}{ms^2+bs} \underbrace{\frac{\omega_1^2(s^2+d_1s+v_1^2)}{v_1^2(s^2+c_1s+\omega_1^2)}}_{\text{first mode}} \underbrace{\frac{\omega_2^2(s^2+d_2s+v_2^2)}{v_2^2(s^2+c_2s+\omega_2^2)}}_{\text{second mode}} \quad (1)$$

From this, ten parameters are necessary to model the interface with two vibration modes. Following an approach similar to the one presented in [23], these parameters could be related to the ten parameters depicted in Fig. 4 for a physical interpretation. Using that nomenclature, it is possible to see that m_1 exactly corresponds to the inertia of the rotor, which is the place where motor's force F actuates and where the encoder measures the device's position X. Coefficients k_{12} and b_{12} model the transmission cable, and k_{23} and b_{23} model a structural mode of the mechanism. However, the ten parameters presented in (1) are more convenient for the identification process.

Parameters of $G(s)$ can be fit manually or by using least-square iterative methods to match the experimental data. Table I reports the obtained parameters, and Fig. 3 depicts the discrete-time Bode diagram for $G(s)$ together with the experimental response. Although only two vibration modes have been modeled, it is clear that the theoretical transfer function properly models the dynamics of the device.

III. Theoretical Stability Boundaries

The system model proposed in the previous section was used to obtain the theoretical stability boundaries of the haptic interaction. A block diagram of the haptic device colliding with a virtual wall is shown in Fig. 5.

Transfer function $G(s)$ is the theoretical model for the device with two vibration modes (1). To be consistent with

TABLE I
PHYSICAL PARAMETERS OF THE PHANToM

Parameter	Variable	Value
Inertia	m	1.168 gm^2
Damping	b	0.00584 Nms/rad
Natural frequency	ω_1	479.166 rad/s
Damping coefficient	c_1	83 rad/s
Natural frequency	v_1	417.612 rad/s
Damping coefficient	d_1	80 rad/s
Natural frequency	ω_2	1159.31 rad/s
Damping coefficient	c_2	352 rad/s
Natural frequency	v_2	546.626 rad/s
Damping coefficient	d_2	90 rad/s

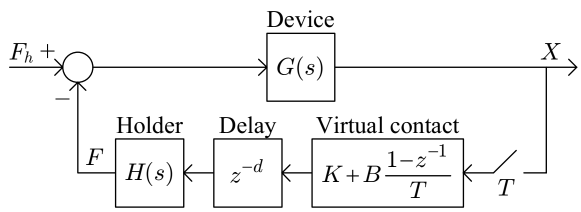

Fig. 5. Block diagram of the impedance haptic rendering.

the acquisition rate of the control board, the sampling period T was set to 1 ms. The impedance of the virtual contact consisted of a virtual stiffness K and a virtual damping B. Before the zero-order holder $H(s)$, a discrete time delay z^{-d} was included to obtain several stability regions with the same device, as it was performed in [24]. Furthermore, the presence of time delay makes the model more complete, since actual haptic systems always suffer from a certain inherent delay due to computation or amplification processes.

The characteristic equation of the system is

$$1 + z^{-d}\left(K + B\frac{1-z^{-1}}{T}\right)\mathcal{Z}[H(s)G(s)] = 0, \quad (2)$$

$$1 + K\frac{\mathcal{Z}[H(s)G(s)]}{z^{d} + B\frac{1-z^{-1}}{T}\mathcal{Z}[H(s)G(s)]} = 0, \quad (3)$$

where $\mathcal{Z}[.]$ is the $\mathcal{Z}$-transform of the transfer function within brackets. The critical stiffness K_{CR}—as a function of the virtual damping and the time delay—can be found by calculating

$$K_{CR} = \mathrm{Gm}\left\{\frac{\mathcal{Z}[H(s)G(s)]}{z^{d} + B\frac{1-z^{-1}}{T}\mathcal{Z}[H(s)G(s)]}\right\}, \quad (4)$$

where Gm$\{.\}$ is the gain margin of the transfer function.

Stability regions can be found for different time delay conditions by computing (4) over a range of virtual damping values. The results for three different time delays ($t_d = 2$, 4 and 8 ms) are shown in Fig. 6. As an example, the Matlab® code to obtain the stability boundary of the PHANToM for a delay of 2 ms is reported in Appendix I.

Notice in Fig. 6 that two different parts can be clearly distinguished for each delay. For small values of virtual damping (part I), the critical stiffness increases with B up to a maximum value $K_{CR}^{\max}$ for B_t. However, for virtual damping coefficients higher than B_t (part II), the critical stiffness

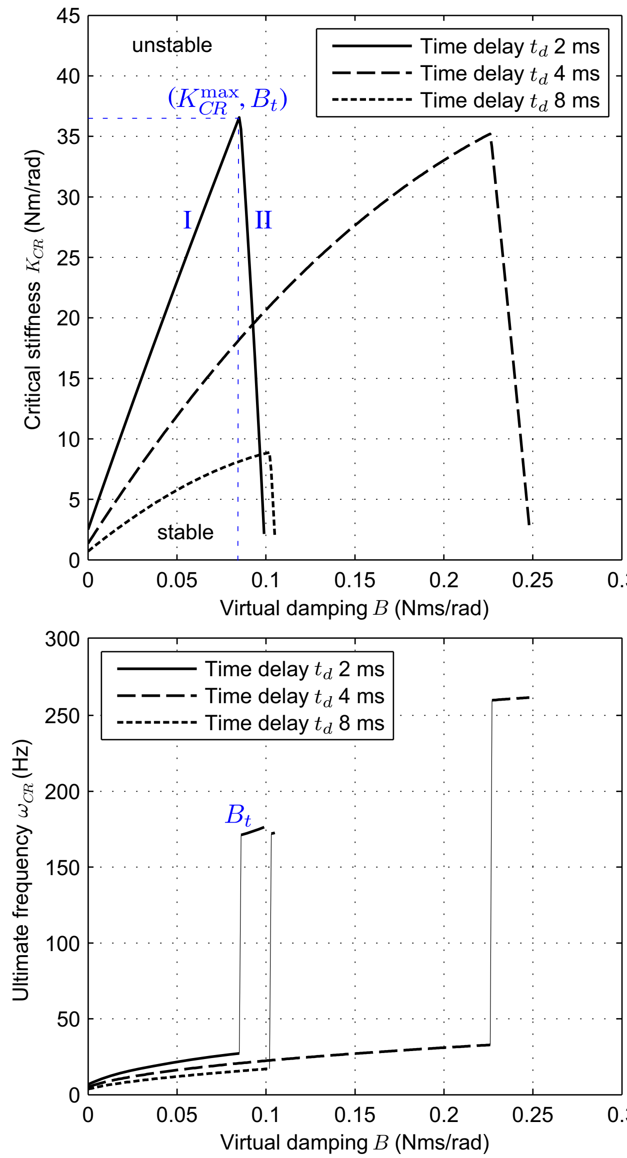

Fig. 6. Critical stiffness (top) and ultimate frequencies (bottom) depending on virtual damping for different time delays.

decreases with B. Therefore, the well known assertion that the virtual damping positively contributes to the stability of the system [8], [10] is true, but limited to a specific range of values.

The critical frequencies of the system for each delay are also reported at the bottom of Fig. 6. The abrupt truncation of the stability region after transition point B_t (part II) occurs when the critical oscillation frequencies jump to higher values. The critical frequency (called "ultimate frequency" from here on) corresponds to the phase crossover frequency of the Bode diagram of transfer function within brackets in (4), which varies with the virtual damping and time delay.

It is interesting to note that the stability region does not always decrease with the delay in the loop. In theory, as stated in [12], the stability region becomes smaller if the time delay increases. However, the stability region with a

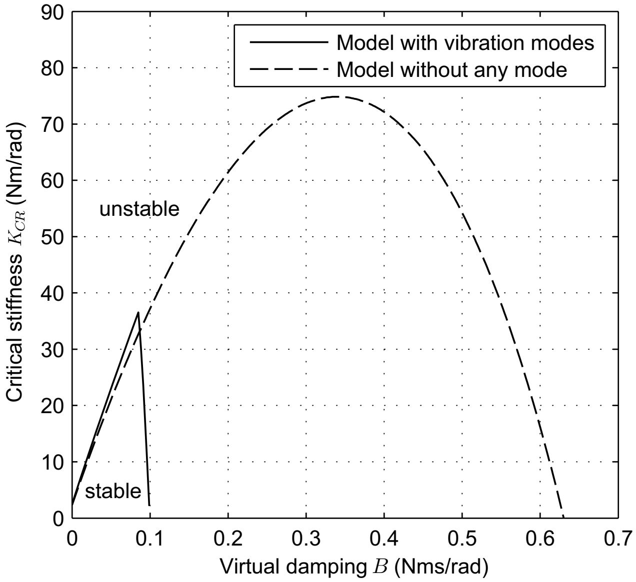

Fig. 7. Critical stiffness using the model with vibration modes (solid line) and without any vibration mode (dashed line) for the same delay of 2 ms.

time delay of 4 ms is larger than the stability region with 2 ms (Fig. 6 top). This unexpected result will be corroborated experimentally in Section IV. The explanation of this behavior cannot be, among others, neither the saturation of the actuator nor the sensor quantization, because the theoretical linear model does not include those limitations. Although the actual reason is not investigated in this study, it seems to be related with the fact that the transition point B_t sometimes reaches a frequency level above the first vibration mode (with time delays of 2 and 8 ms), and other times above the second vibration mode (time delay of 4 ms).

Related work [17], [18], [22] has previously found experimentally that for large values of virtual damping, the critical stiffness of the system decays abruptly. The haptic model proposed in this paper has included two vibration modes in order to find the theoretical explanation for this phenomenon and depict the stable region much more accurately. Fig. 7 shows the stability regions obtained using the theoretical model with and without vibration modes. In both cases, the delay was set to 2 ms. The vibration modes of the interface impose an important restriction in the Z-width of the PHANToM. Notice that the influence of the vibration modes also affected part I of the boundary: in this case, the critical stiffness was higher when the vibration modes were included.

IV. Experimental Stability Boundary

The critical values for the virtual stiffness of the PHANToM were experimentally obtained to validate the theoretical boundaries shown in the previous section. The critical limits were found by using the relay method [10], [25], [26]. This method consists of a relay feedback—an on-off controller—that makes the system oscillate around a reference position. In steady state, the relay force is a square wave, the output position is similar to a sinusoid wave, and they have opposite phases (Fig. 8). It can be demonstrated [25] that the ultimate frequency ω_{CR} is the oscillation frequency of both signals, and the critical gain is the quotient of the amplitudes of the first harmonic of the square wave and the output position. The oscillation frequency is found by determining the maximum peak of the average power spectral density of both signals in steady state. The gain margin is obtained by evaluating the empirical transfer function (*tfestimate* Matlab® function using input-output signals) at the oscillation frequency.

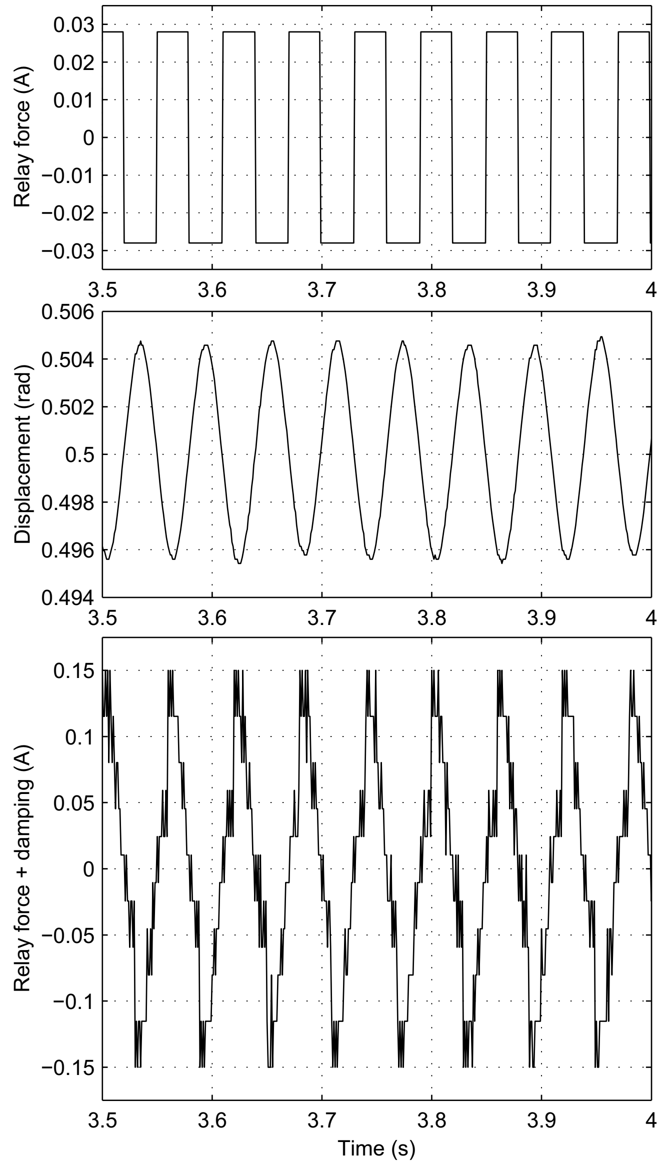

Fig. 8. Recorded input and output signals during a relay experiment with time delay $t_d = 8$ ms and virtual damping $B = 0.08$ Nms/rad.

The testbed description and kinematic configuration are the same as in Section II. The reference for the relay force transition was placed approximately at the middle of the available workspace. Input force was applied to the active motor, and the position of the device was measured. In each relay experiment, all signals were measured for more than

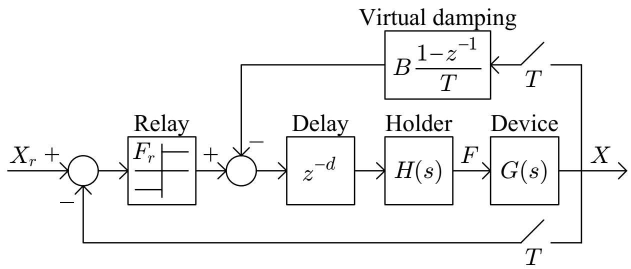

Fig. 9. Block diagram of the relay experiment.

TABLE II
CRITICAL OSCILLATIONS FOR THE PHANToM

t_d (ms)	B (Nms/rad)	K_{CR} (Nm/rad)	ω_{CR} (Hz)	t_d (ms)	B (Nms/rad)	K_{CR} (Nm/rad)	ω_{CR} (Hz)
2	0	7.21	13.61	4	0	1.97	6.79
2	0.03	17.06	20.38	4	0.05	13.55	17.99
2	0.05	24.23	24.38	4	0.05	18.92	21.59
2	0.08	33.81	28.54	4	0.5	21.95	23.59
2	0.1	40	30.54	4	0.15	28.25	27.59
2	0.11	3.29	188	4	0.18	31.77	29.59
2	0.12	3.07	187	4	0.2	34.09	31.19
8	0	1.01	4.7	4	0.23	37.71	32.79
8	0.05	6.37	13.2	4	0.25	39.09	32.79
8	0.08	7.88	15.97	4	0.254	40.23	33.19
8	0.1	9.78	17.9	4	0.264	23.81	266
8	0.13	10.32	20.6	4	0.27	23.19	266
8	0.14	3.24	177	4	0.3	15	266

15 seconds (in steady state).

To obtain the critical values for different damping coefficients and delays, the relay force was not directly commanded to the device. The viscous force due to the virtual damping was added to the relay force, and then both of them were delayed (Fig. 9 bottom). This way, the relay method obtained the critical gain (4).

As in previous section, time delay was artificially set to 2, 4 and 8 ms. Without any delay in the loop, it is not possible to obtain the complete stability region experimentally because the actuator becomes saturated. Table II and Fig. 10 present the oscillation frequencies and gain margins of the 26 experiments performed. Fig. 10 shows that the theoretical results depicted in Fig. 6 fit quite well with the experimental data. This data allows the two parts of the stability region to be identified and shows the truncation of the boundary at a certain damping value.

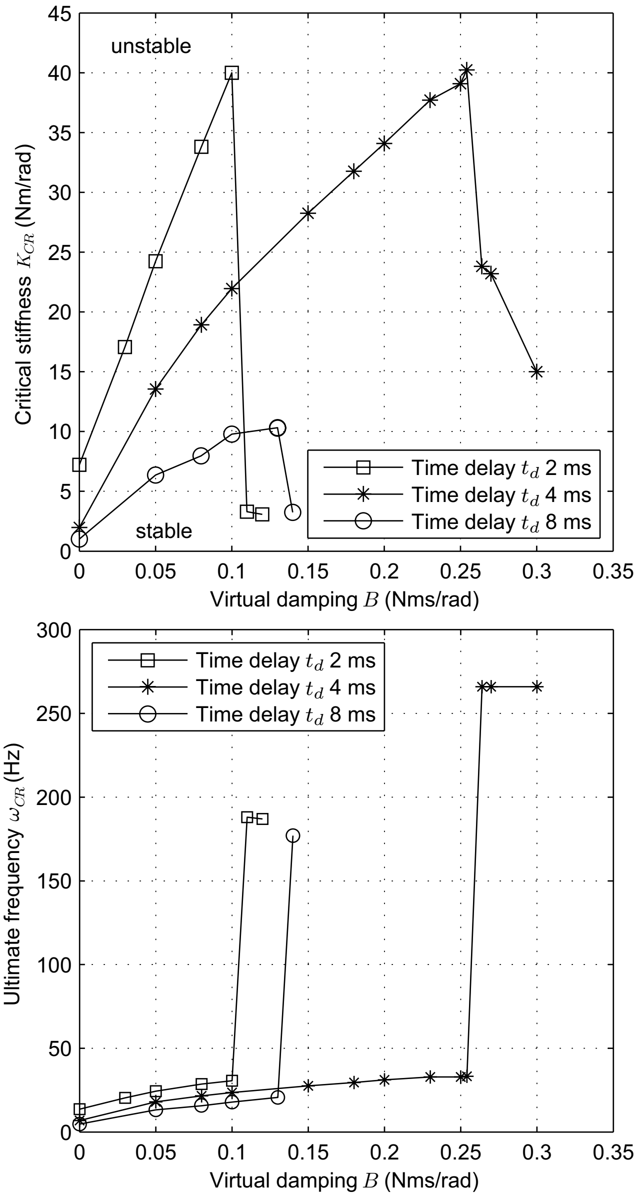

Fig. 10. Critical stiffness (top) and ultimate frequencies (bottom) as a function of the virtual damping for different time delays.

V. CONCLUSIONS AND FUTURE WORK

This paper presents the basis for a better understanding of the influence of the vibration modes on the Z-width of a haptic system, that is, the set of stable parameters that can be simulated—usually a (K, B) pair. The theoretical and experimental results confirm that the vibration modes of the mechanical interface drastically decrease the Z-width of the system, and impose an upper limit on the virtual damping coefficient B that can be implemented.

The existence of this limit was already known experimentally in the field of haptics. Several authors [17], [18], [22] had found the stability regions of different haptic devices, showing the abrupt truncation of the Z-width of the system at a certain damping point. However, none of them could predict the shape of the boundary a priori. Although this paper does not provide a theoretical expression for the maximum achievable damping coefficient B, it has demonstrated the possibility of numerically determining the stability boundaries for one degree-of-freedom of the PHANToM 1.0 haptic interface. To obtain this result, a linear transfer function with two vibration modes was identified.

Future work will more deeply investigate the effect of time delays in the Z-width limitation due to vibration modes, and more specifically why the system changes its ultimate vibration frequency with delays will be analyzed. The theoretical analysis and results will also be extended to other devices and kinematic configurations.

APPENDIX I

Matlab® code used to depict the stability region (Fig. 6) of the PHANToM with 2 ms of delay:

```
G0=tf(856,[1 5 0]);
G1=tf(2296*[1 80 174400],1744*[1 83 229600]);
G2=tf(13440*[1 90 298800],2988*[1 352 1344000]);
G=G0*G1*G2;
T=0.001;
z=tf([1 0],1,T);
Gz=c2d(G,T);
vector=0:0.001:0.099;
K2ms=vector*0;
W2ms=vector*0;
n=0;
for B=vector,
  n=n+1;
  [Q,F,WQ,WF]=margin(T/(((T*z*z)/Gz)+B*(z-1)/z));
  K2ms(n)=Q;
  W2ms(n)=WQ/(2*pi);
end
B=vector;
plot(B,K2ms);
figure;
plot(B,W2ms);
```

REFERENCES

[1] P.-A. Heng, C.-Y. Cheng, T.-T. Wong, Y. Xu, Y.-P. Chui, K.-M. Chan, and S.-K. Tso, "A virtual-reality training system for knee arthroscopic surgery," *IEEE T. Inf. Technol. Biomed.*, vol. 8, no. 2, pp. 217–227, June 2004.

[2] M. Li and Y.-H. Liu, "Haptic modeling and experimental validation for interactive endodontic simulation," in *IEEE Int. Conf. Robot. Autom.*, Orlando, Florida, USA, May 15-19 2006, pp. 3292–3297.

[3] J. Savall, D. Borro, J. J. Gil, and L. Matey, "Description of a haptic system for virtual maintainability in aeronautics," in *2002 IEEE/RSJ Int. Conf. on Intelligent Robots and Systems*, Lausanne, Switzerland, September 30 - October 5 2002, pp. 2887–2892.

[4] M. Bergamasco, A. Frisoli, and F. Barbagli, "Haptics technologies and cultural heritage applications," in *Computer Animation*, 2002, pp. 25–32.

[5] J. E. Colgate and G. Schenkel, "Passivity of a class of sampled-data systems: Application to haptic interfaces," *J. Robot. Syst.*, vol. 14, no. 1, pp. 37–47, January 1997.

[6] J. J. Abbott and A. M. Okamura, "Effects of position quantization and sampling rate on virtual-wall passivity," *IEEE Trans. Robot.*, vol. 21, no. 5, pp. 952–964, October 2005.

[7] N. Diolaiti, G. Niemeyer, F. Barbagli, and J. K. Salisbury, "Stability of haptic rendering: Discretization, quantization, time-delay and coulomb effects," *IEEE Trans. Robot.*, vol. 22, no. 2, pp. 256–268, April 2006.

[8] M. Minsky, M. Ouh-young, O. Steele, F. Brooks Jr., and M. Behensky, "Feeling and sensing: Issues in force display," *Computer Graphics*, vol. 24, no. 2, pp. 235–243, March 1990.

[9] S. E. Salcudean and T. D. Vlaar, "On the emulation of stiff walls and static friction with a magnetically levitated input/output device," *Journal of Dynamics, Measurement and Control*, vol. 119, pp. 127–132, March 1997.

[10] J. J. Gil, A. Avello, A. Rubio, and J. Flórez, "Stability analysis of a 1 dof haptic interface using the routh-hurwitz criterion," *IEEE Trans. Control Syst. Technol.*, vol. 12, no. 4, pp. 583–588, July 2004.

[11] T. Hulin, C. Preusche, and G. Hirzinger, "Stability boundary for haptic rendering: Influence of physical damping," in *2006 IEEE/RSJ Int. Conf. on Intelligent Robots and Systems*, Beijing, China, October 9-15 2006, pp. 1570–1575.

[12] J. J. Gil, E. Sánchez, T. Hulin, C. Preusche, and G. Hirzinger, "Stability boundary for haptic rendering: Influence of damping and delay," in *IEEE Int. Conf. Robot. Autom.*, Roma, Italy, April 10-14 2007, pp. 124–129.

[13] J. S. Mehling, J. E. Colgate, and M. A. Peshkin, "Increasing the impedance range of a haptic display by adding electrical damping," in *WorldHaptics Conf.*, Pisa, Italy, 18-20 March 2005, pp. 257–262.

[14] A. H. Gosline, G. Campion, and V. Hayward, "On the use of eddy current brakes as tunable, fast turn-on viscous dampers for haptic rendering," in *EuroHaptics 2006*, Paris, France, July 3-6 2006, pp. 229–234.

[15] D. W. Weir, J. E. Colgate, and M. A. Peshkin, "Measuring and increasing z-width with active electrical damping," in *16th Int. Symp. Haptic Interfaces Virtual Environ., Teleoper. Syst.*, Reno, NV, USA, March 13-14 2008, pp. 169–175.

[16] Y.-A. Lim, H. S. Ahn, and J. Ryu, "Performance of equivalent frequency-dependent damping," in *WorldHaptics Conf.*, Salt Lake City, UT, USA, March 18-20 2009, pp. 559–564.

[17] J. E. Colgate and J. M. Brown, "Factors affecting the z-width of a haptic display," in *1994 IEEE Int. Conf. Robot. Autom.*, vol. 4, San Diego, CA, USA, 1994, pp. 3205–3210.

[18] F. Janabi-Sharifi, V. Hayward, and C.-S. J. Chen, "Discrete-time adaptive windowing for velocity estimation," *IEEE Trans. Control Syst. Technol.*, vol. 8, no. 6, pp. 1003–1009, November 2000.

[19] J.-H. Ryu, C. Preusche, B. Hannaford, and G. Hirzinger, "Time domain passivity control with reference energy following," *IEEE Trans. Control Syst. Technol.*, vol. 13, no. 5, pp. 737–742, September 2005.

[20] J. Artigas, J. Vilanova, C. Preusche, and G. Hirzinger, "Time domain passivity control-based telepresence with time delay," in *2006 IEEE/RSJ Int. Conf. on Intelligent Robots and Systems*, Beijing, China, October 9-15 2006.

[21] D. Ryu, J.-B. Song, J. Choi, S. Kang, and M. Kim, "Frequency domain stability observer and active damping control for stable haptic interaction," in *2007 IEEE Int. Conf. Robot. Autom.*, Roma, Italy, April 10-14 2007, pp. 105–110.

[22] N. Yasrebi and D. Constantinescu, "Extending the z-width of a haptic device using acceleration feedback," in *EuroHaptics 2008*, Madrid, Spain, June 11-13 2008, pp. 157–162.

[23] I. Díaz and J. J. Gil, "Influence of vibration modes and human operator on the stability of haptic rendering," *IEEE Trans. Robot.*, vol. 26, no. 1, pp. 160–165, February 2010.

[24] J. J. Gil, E. Sánchez, T. Hulin, C. Preusche, and G. Hirzinger, "Stability boundary for haptic rendering: Influence of damping and delay," *J. Comput. Inf. Sci. Eng.*, vol. 9, no. 1, p. 011005, March 2009.

[25] K. J. Åström and T. Hägglund, *PID Controllers: Theory, Design, and Tuning*. North Carolina: Instrument Society of America, 1995.

[26] L. Barbé, B. Bayle, and M. de Mathelin, "Towards the autotuning of force-feedback teleoperators," in *8th Int. IFAC Symposium on Robot Control*, Bologna, Italy, September 6-8 2006.